J Solid State Electrochem (2010) 14:1197–1204
DOI 10.1007/s10008-009-0948-5

ORIGINAL PAPER

Evaluation of passive film behaviour of super austenitic stainless steels at different potential regions using dynamic electrochemical impedance spectroscopy

S. Nagarajan · V. Raman · N. Rajendran

Received: 3 August 2009 / Revised: 8 September 2009 / Accepted: 5 October 2009 / Published online: 27 October 2009

Abstract Potentiodynamic anodic polarisation and dynamic electrochemical impedance spectroscopic (DEIS) measurements were carried out on 316L stainless steel and alloys 926 and 31 in natural seawater in order to assess the crevice corrosion resistance. DEIS measurements were performed over a wide range of potentials covering the corrosion potential, passive region, breakdown region and dissolution region. The impedance measurements in potentiodynamic conditions clearly reveal the changes that occur in the passive layer with change in potential. The impedance spectra at different potential regions were also discussed elaborately. The surface morphology of the alloy after crevice corrosion was studied using optical microscope and atomic force microscopy.

Keywords Stainless steel · Crevice corrosion · Dynamic electrochemical impedance spectroscopy · Atomic force microscopy

Introduction

Crevice corrosion is one of the most serious problems when stainless steel (SS) is used in chloride environments, which is often very difficult to control. This form of corrosion on SS is considered to initiate via a gradual build up of acidity within the crevice. The various stages in which this occurs are as follows: depletion of oxygen in the crevice makes it a net anode; metal ions produced by passive dissolution within the crevice are only transported away slowly due to the hydrolysis of these ions which leads to an increase in the acidity within the crevice area. To ensure electroneutrality, the anions migrate into the crevice, and eventually, the crevice solution becomes sufficiently aggressive to depassivate the metal surface, i.e. initiate crevice corrosion [1–4].

In order to avoid such type of corrosion, counter measures such as structural modifications, reducing the aggressiveness of the environment and materials selection, have been tried earlier. The selection of materials with sufficient resistance to crevice corrosion in the given environments has also been developed. Many researchers have reported that SS containing high alloying elements such as Cr, Mo and N are used to improve the crevice corrosion resistance [5, 6]. Bond and Dundas [7] conducted the crevice corrosion test for commercial SS and found that high Cr and Mo containing ferritic SS possess superior corrosion resistance than austenitic SS. A strong correlation between pitting corrosion and crevice corrosion mechanism was reported by Wilde and William for some metal-environment systems, particularly in NaCl solutions and in seawater [8]. Modelling of pit and crevice corrosion propagation was reviewed and addressed in considerable depth both empirically and also through mechanical modelling [9].

Brigham [10] has proposed the mechanism leading to the initiation of crevice corrosion based on the fundamental thermodynamic and electrochemical principles. Various other crevice corrosion mechanisms have been proposed over the years. Electrochemical impedance measurement performed on the creviced 316L SS leads to the conclusion that the initiation stage of crevice corrosion in chloride environments is similar to that for the initiation of pitting corrosion [11].

S. Nagarajan · V. Raman · N. Rajendran (✉)
Department of Chemistry, Anna University Chennai, Chennai, India
e-mail: nrajendran@annauniv.edu

During the crevice corrosion process, the nature of the passive film on the metal surface may be varied with respect to its environment. In such a case, the stationary condition for the investigated system is not fulfilled, and the classical EIS fails. This disadvantage in using the classical EIS technique initiate us to carry out dynamic electrochemical impedance spectroscopy (DEIS), which can possibly follow the passive layer changes on the metal surface during the crevice corrosion process. Darowicki et al. [12–15] developed the dynamic electrochemical impedance technique and investigated the pitting corrosion, pit pre-initiation state and transports of organic coatings. Hence, the objective of this study is to understand the passive film behaviour of 316L SS, alloy 926 and alloy 31 in natural seawater environment under the influence of changes in the electrode potential.

Experimental

The chemical compositions of the 316L SS and alloys 926 and 31 are given in Table 1. Bars of dimensions 50×50×3 mm with 10 mm hole in the centre were cut out and wet-polished with emery paper up to 600. The specimens were then washed with distilled water, degreased with acetone followed by alcohol and dried. Multi-crevice corrosion test assembly was prepared based on the standard guide for crevice corrosion test, ASTM G78. The crevice former was a polyacetal resin rings, which had 20 teeth of dimensions 2×2 mm; two of these rings were pressed onto the specimen at a torques of 8.5 Nm with titanium bolt and a nut, so that 20 small crevice sites were formed on each side of the specimen. The bolt was electrically insulated from the specimens using a polytetrafluoroethylene tape. The multi-crevice assembly thus obtained were immersed in the electrolyte. A conventional three-electrode cell was used for all the electrochemical measurements. A saturated calomel electrode (SCE) was used as a reference electrode, platinum foil as a counter electrode and the test material as the working electrode. Natural seawater collected from the coastal area of Chennai, India, served as the electrolyte.

Potentiodynamic cyclic polarisation studies were carried out for the test specimens in natural seawater. The potentiostat (model PGSTAT 12, AUTOLAB, The Netherlands B.V) was controlled by a personal computer. A dedicated software (GPES version 4.5) was used for conducting the polarisation experiments. The potential was applied on the working electrode at a scan rate of 0.167 mV s^{-1}. In order to test the reproducibility, the experiments were performed in triplicate.

DEIS measurements were carried out using a frequency response analyser (FRA), which included a potentiostat model PGSTAT 12. Impedance spectra were acquired from the corrosion potential to the dissolution region with a step potential of 20 mV in the frequency range of 55 kHz–0.1 Hz with a 10-mV amplitude sine wave generated by the FRA.

The surface morphology was recorded by atomic force microscopy (AFM) using a Nanosurf easy scan 2 (Nanosurf AG, Grammetstrasse 14, 4410 Liestal, Switzerland). The images were acquired by contact mode, using silicon nitride cantilevers with a spring constant of 0.15 N/m at a resonance frequency of 13 kHz. All images were recorded under air atmosphere at room temperature.

Table 1 Chemical composition of investigated alloys (wt.%)

Alloy	Main alloying elements (wt.%)					
	Cr	Ni	Mo	N	C	Mn
316L SS	17.2	12.6	2.4	0.02	0.030	1.95
Alloy 926	21.0	25.0	6.5	0.20	0.003	1.95
Alloy 31	27.0	31.0	6.5	0.20	0.003	0.68

Results and discussion

Potentiodynamic polarisation studies

The anodic polarisation curves of the three specimens viz type 316L SS, alloy 926 and alloy 31 is given in Fig. 1. The corrosion potentials for the alloys were observed at −300, −238 and −197 mV vs SCE, respectively, in natural seawater. Compared to the 316L SS, the corrosion potential values of alloy 926 and alloy 31 were shifted to nobler region, due to the presence of higher amounts of nickel, molybdenum, chromium and nitrogen.

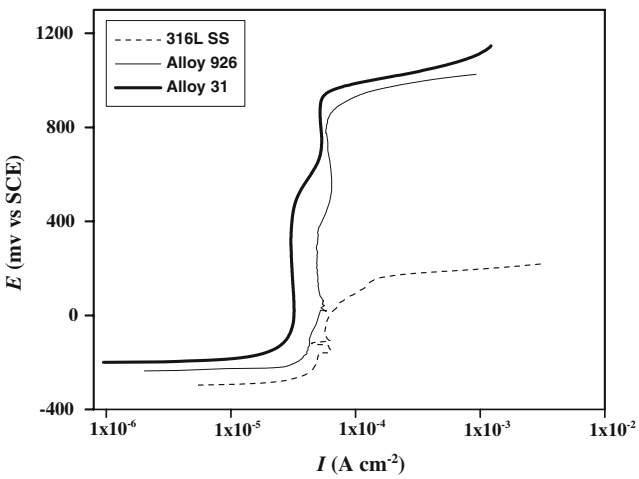

Fig. 1 Potentiodynamic polarisation curves for 316L SS, alloy 926 and alloy 31 in natural seawater

Crevice potential of the materials is the criterion for evaluating resistance to crevice attack, which is directly influenced by the amount of passivating elements present in the alloy. The critical crevice potential for the type 316L SS was 133 mV, whereas for alloy 926 and alloy 31, the critical crevice potentials were observed at 936 and 989 mV, respectively. Thus, alloy 926 and alloy 31 exhibits better crevice corrosion resistance in the natural seawater compared to reference material 316L SS.

The observed increase in crevice corrosion resistance of the super austenitic SS can be explained based on the following postulates. During active dissolution, nickel and chromium were generally dissolved, whereas non-active elements such as nitrogen were enrich at the surface. Such an enrichment of the passive film inhibits the anodic dissolution of the materials by two orders of magnitude, presumably through the formation of iron nitride. The presence of iron nitride inhibits the autocatalytic process of pit formation and also it helps in the healing of the already formed pit. Thus, addition of small amounts of nitrogen can enhance the crevice resistance and passivation characteristics [16–19]. It is believed that the nitrogen in the steel dissolves; it consumes protons in the pit to form ammonia, thus preventing the lowering of the pH within the pit, which contributes to the suppression of acidification inside the pit. It is also speculated that surface films are stabilised through passivation or nitrogen enrichment at the film/metal interface to prevent the attack of the chloride anions [20].

A synergistic influence of nitrogen and molybdenum on pitting and crevice corrosion resistance at the surface has been reported earlier [21]. Newman et al. [22] reported that enrichment of nitrogen and molybdenum at the interface is the predominant factor for preventing further dissolution of the substrate consequent to the destruction of the passive film.

Potentiodynamic impedance spectroscopic studies

The impedance spectra were obtained for every 20-mV increase in the potential, beginning from the open-circuit potential (OCP) to the dissolution potential. Figure 2a–c shows that three-dimensional representations of all the impedance spectra of 316L SS, alloys 926 and 31 were obtained from the potentiodynamic impedance studies. A linear increase in the magnitude of impedance was observed from OCP irrespective of the alloy. In the case of 316L SS, the impedance values increases with potential and attains a maximum around 110 mV. Further increase in potential causes a sudden decrease in the impedance values. However, in the case of alloys 926 and 31, the magnitude of impedance attained a maximum value approximately at 180 and 140 mV, respectively. Further increase in the potential results in the decrease of the impedance values up to a certain extent and then the magnitude of impedance increases. The results obtained from DEIS, when correlated with polarisation curves of 316L SS, alloys 926 and 31,

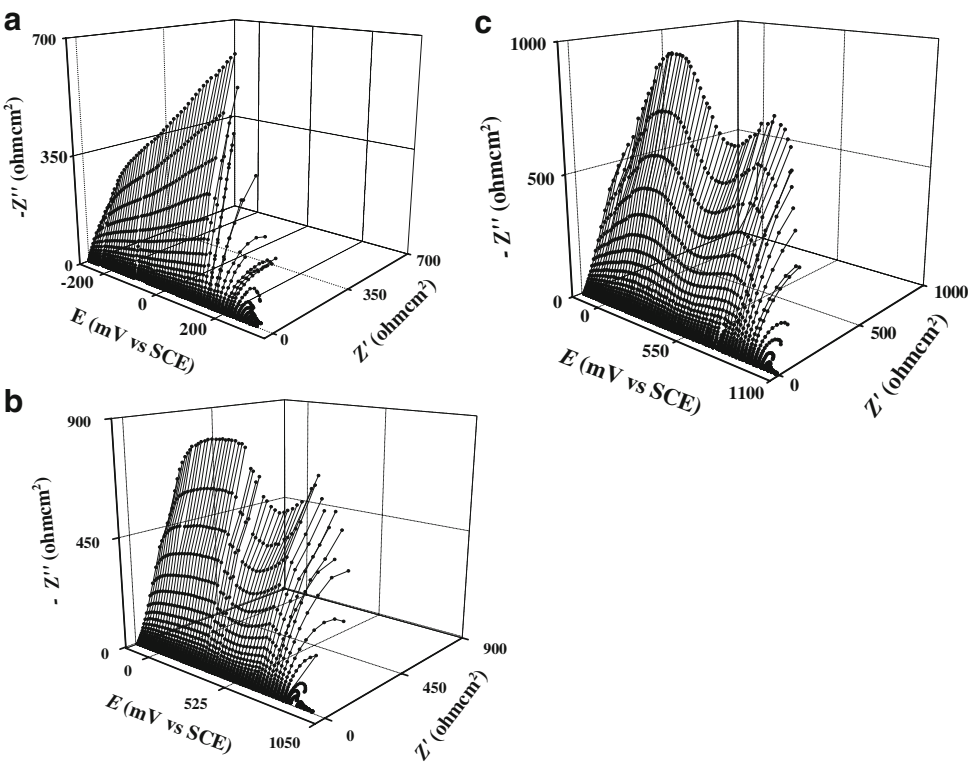

Fig. 2 The impedance versus potential diagram of (**a**) 316L SS, (**b**) alloy 926 and (**c**) alloy 31

revealed a precise information on the passive film behaviour from OCP till dissolution potential. For instance, firstly, all the alloys exhibited a maximum resistance before breakdown. Though polarisation curves also depicted the same, the result obtained from DEIS was more apparent. Secondly, in the case of alloys 926 and 31, the decline in the value before the secondary maxima, essentially due to the thinning of the passive film, was not clearly visible from the polarisation curves. Thirdly, the breakdown potentials can also be determined precisely using DEIS compared to the polarisation studies.

In order to have a better understanding of the crevice corrosion process, electrochemical impedance spectra was obtained at selected regions: OCP, passive, breakdown and dissolution. Figure 3a–c shows the Nyquist plots at OCP, and Fig. 4a–c shows the Nyquist plots in the passive region for 316L SS, alloys 926 and 31, respectively. All the spectra exhibited a similar behaviour containing a straight line with a high magnitude of impedance, which indicates a highly resistant passive film. This is in good agreement with the earlier report [23].

Figure 5a–c shows the impedance spectra of the alloys at the breakdown potential. The reference material 316L SS exhibited a two-time constant. However, for alloys 926 and

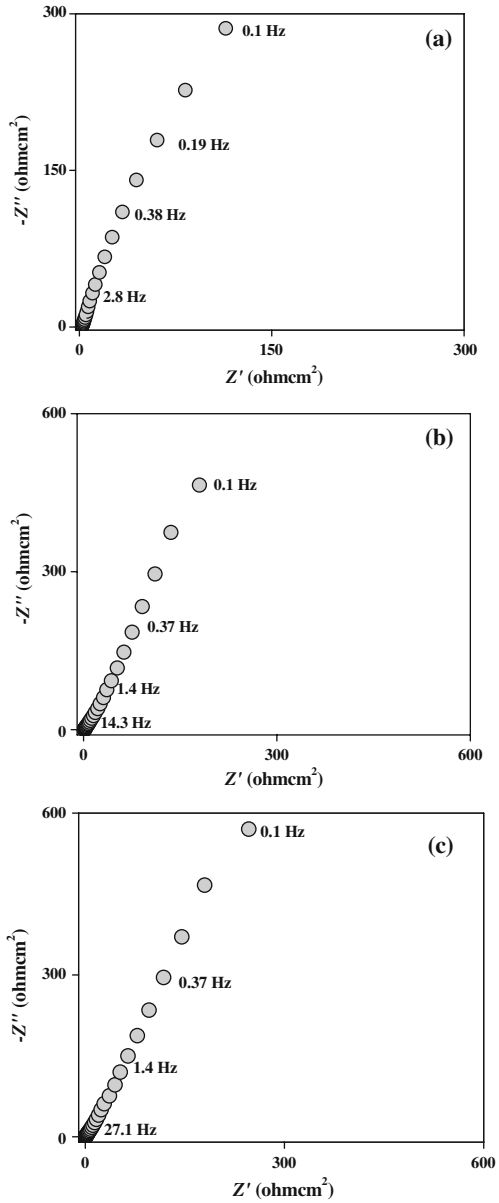

Fig. 3 Nyquist plot at open-circuit potential for (**a**) 316L SS, (**b**) alloy 926 and (**c**) alloy 31

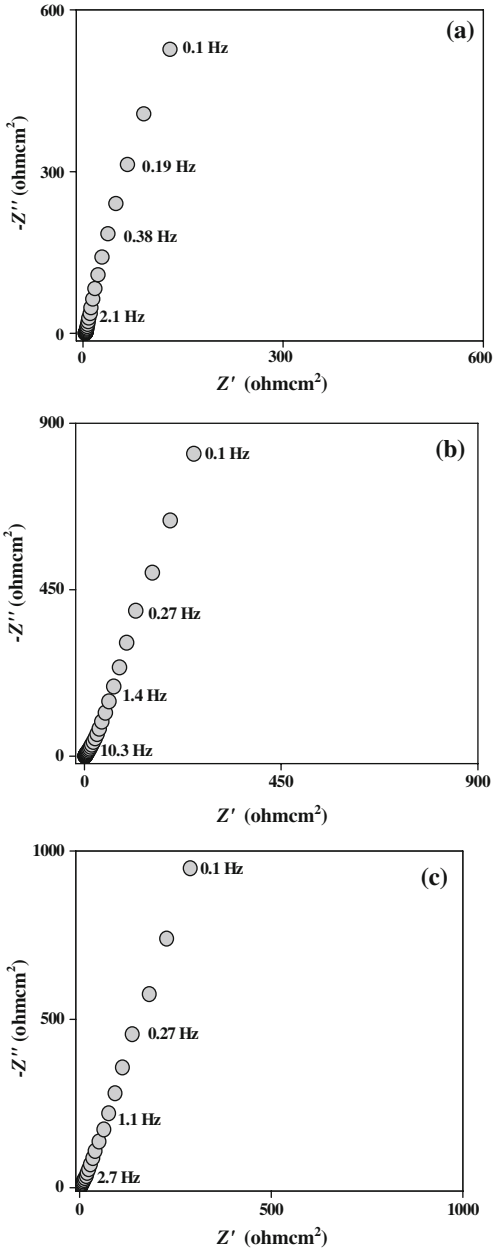

Fig. 4 Nyquist plot at passive region for (**a**) 316L SS, (**b**) alloy 926 and (**c**) alloy 31

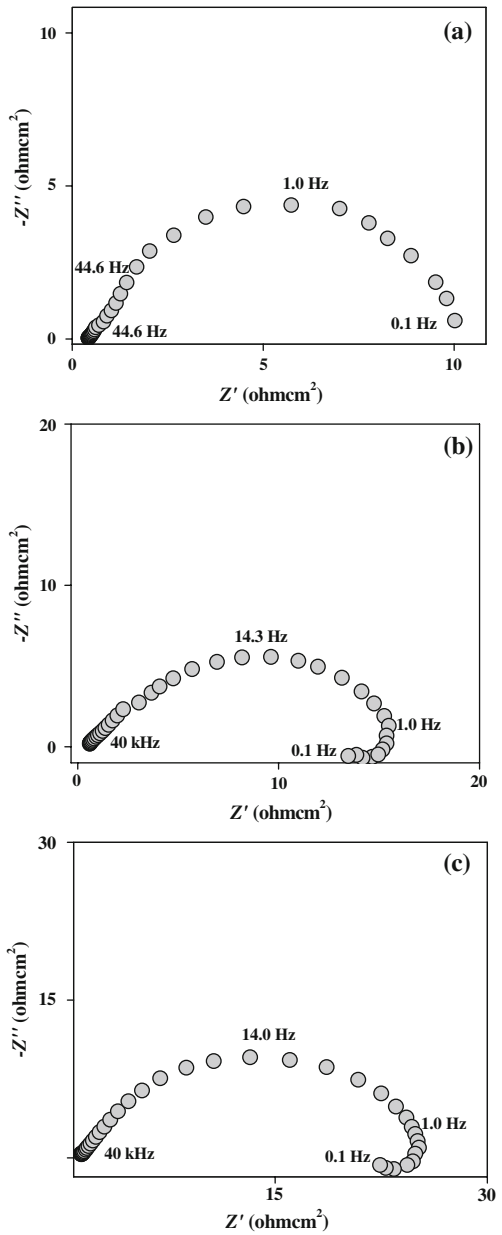

Fig. 5 Nyquist plot at breakdown potential for (**a**) 316L SS, (**b**) alloy 926 and (**c**) alloy 31

31, a two-time constant and also a low-magnitude inductive loop at lower frequency was observed.

The appearance of a capacitive loop in the form of a semicircle for alloys 926 and 31 can be attributed to a charge transfer at the film/solution interface. A fast charge transfer process, which takes place at the interface for all the alloys, was revealed from a very small and depressed high frequency capacitive loop. The inductive loop observed at lower frequency is most probably due to the relaxation process of an intermediate species of the dissolution reaction. Substantial reports are available for the presence of inductive loops in the low frequency range of the impedance spectra obtained for high alloys [24, 25]. Figure 6a–c shows the Nyquist plot of 316L SS, alloys 926 and 31 at the dissolution region. The 316L SS exhibited a semicircle, having lower impedance value with a more pronounced Warburg tail. The Warburg impedance observed may be attributed to an ionic diffusion through the solid corrosion products that precipitated near the pit mouth as reported by Dawson and Ferreira [11]. The Nyquist plot corresponding to alloy 926 at the dissolution region exhibits two capacitive loops at higher frequency and an inductive loop at intermediate frequency, and this was

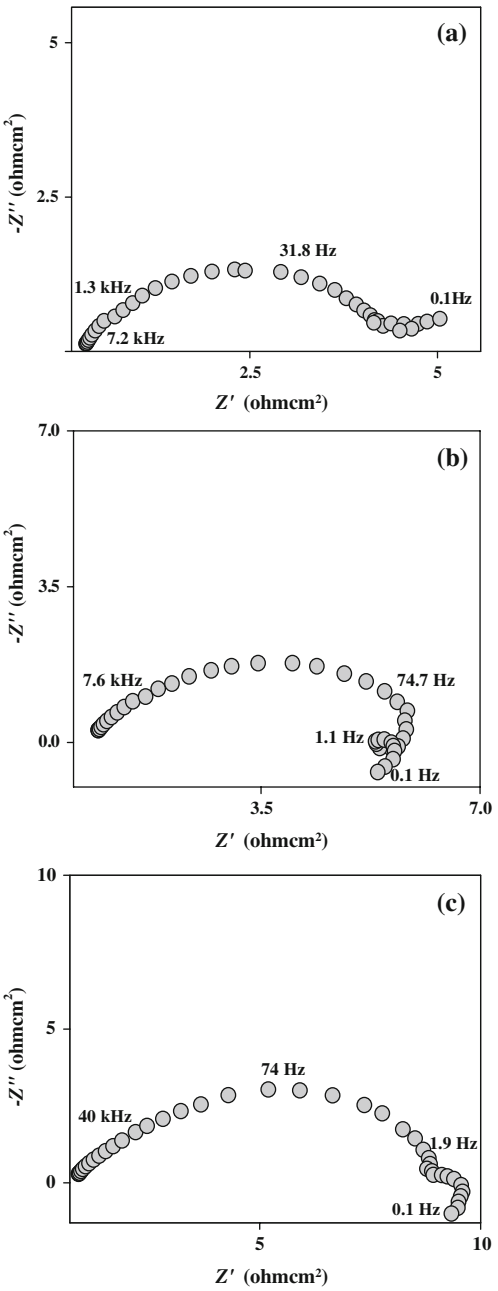

Fig. 6 Nyquist plot at dissolution region for (**a**) 316L SS, (**b**) alloy 926 and (**c**) alloy 31

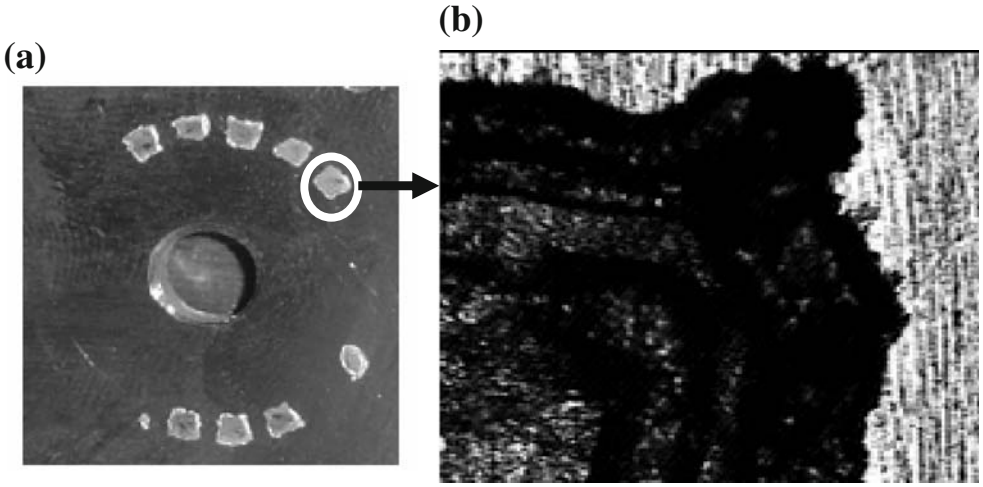

Fig. 7 Surface morphology of 316L SS after crevice corrosion test (**a**) photographs and (**b**) optical micrographs

presumably due to the metal charge transfer and relaxation process of an intermediate species at the film/solution interface, while the low frequency capacitive loop can be assigned to the secondary passivation. The lowest frequency inductive loop obtained was not considered in the subsequent analysis because of the possibility that it was due to the slow process of the system. Whereas in case of alloy 31, two capacitive loops at higher and intermediate frequency regions, another small capacitive loop followed by an inductive loop at lower frequency was observed. The small semicircle at the intermediate frequency can be due to the adsorption effects, and it has been attributed to the increase in the surface coverage of intermediate species formed during metal dissolution. The formation of such intermediate species can be associated with the enhanced crevice corrosion resistance of alloy 31. Further, the very low frequency inductive loop could also be related to an increase in the ionic conductivity of the oxide film with potential. It has been reported that the chloride activity within their crevices increases only very slightly compared to the bulk solution, and it has been proposed that much of the chloride in the crevice must have formed complexes

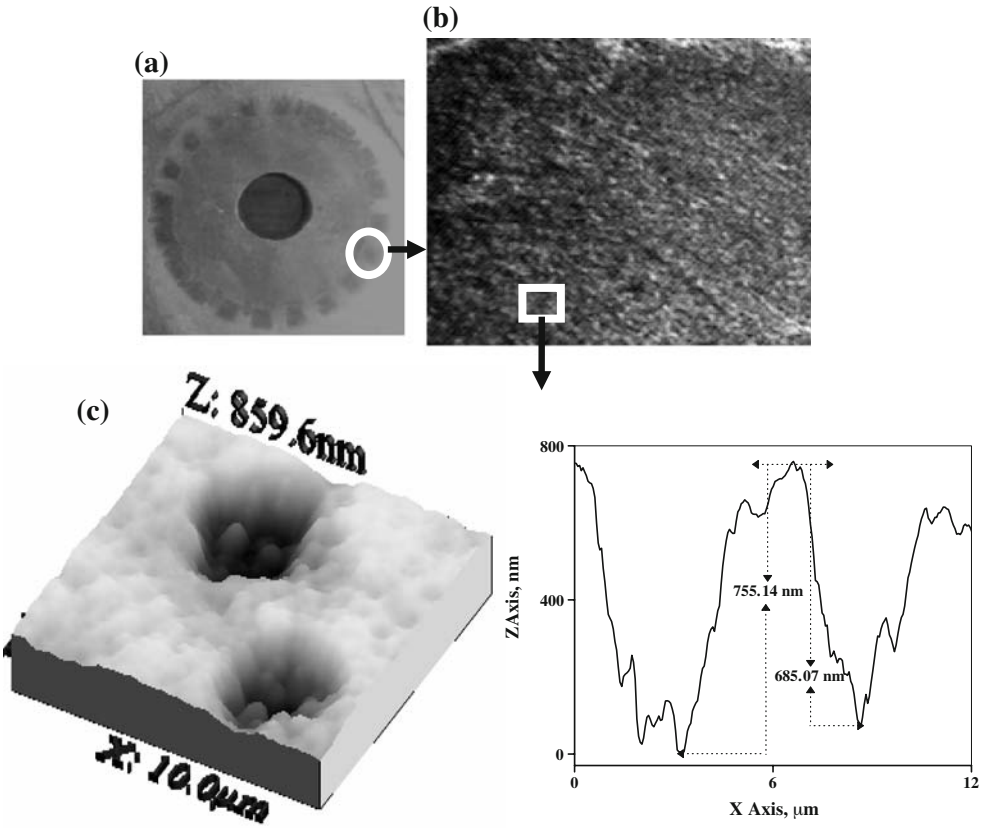

Fig. 8 Surface morphology of alloy 926 after crevice corrosion test (**a**) photographs (**b**) optical micrographs and (**c**) atomic force microscopy images

like $(MOMOHCl)_{ads}$ and $(MOMCl)_{ads}$ with the metal ions, which accelerates metal dissolution [26–28]. The lower frequency inductive loop may be due to the relaxation process of an intermediate species, which takes place at a slower phase [29]. Generally, such slower relaxation processes does not play a significant role in the passivation behaviour. However, alloy 31 and alloy 926 have better crevice corrosion resistance than 316L SS.

Surface characterisation

Figure 7a shows the visual image of 316L SS after crevice corrosion test. The image clearly revealed that a severe damage on the surface of the specimen has taken place due to the crevice corrosion process. In order to get further insight on the crevice corrosion process, optical micrographs were taken at the crevice site and are shown in Fig. 7b. The micrographs exhibited a surface with a few millimetre depth of crevice-affected area. Similar surface characterisation studies were also carried out for alloy 926 and 31 and are shown in Fig. 8a, b and 9a, b, respectively. The optical microscopic image of the alloys 926 and 31 does not give any clear evidence for the crevice corrosion process. In order to probe in further detail, AFM micrographs were taken at the crevice site for these specimens, and the images are given in Figs. 8c and 9c, respectively, for the alloys 926 and 31. This pit appearance is presumably due to a particle-enhanced local dissolution of the matrix at the boundary. The depths of the pit were calculated for these two alloys; alloy 926 exhibited a pit depth of around 720 nm, and alloy 31 exhibited a pit depth around 600 nm. From the pit depth values, it was envisaged that the alloy 31 exhibits better crevice corrosion resistance than the other two alloys viz 926 and 316L SS.

Conclusion

The crevice corrosion resistance observed for alloys 926 and 31 in natural seawater shows higher crevice corrosion resistance compared to that of 316L SS, and this is attributed to the presence of both nitrogen and molybdenum in the super austenitic alloys. The DEIS technique has been used to evaluate the crevice corrosion resistance of alloys 926 and 31 in natural seawater. The Nyquist plot at different potential regions, namely, OCP, passive region, breakdown region and dissolution region, reveals that the impedance changes as a function of potential. The critical crevice potential measured from the polarisation data is in good agreement with the DEIS data. An atomic force microscopic study reveals nano-crevice attack on these alloys even though alloys 926 and 31 exhibits higher crevice corrosion resistance than 316L SS.

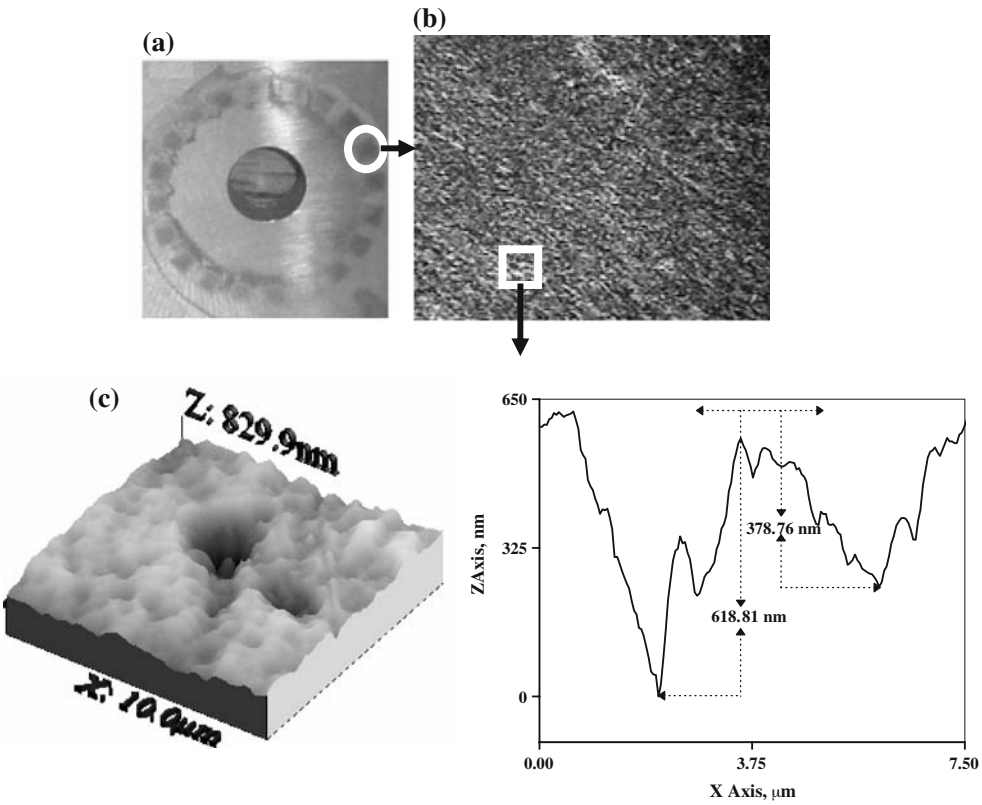

Fig. 9 Surface morphology of alloy 31 after crevice corrosion test (**a**) photographs (**b**) optical micrographs and (**c**) atomic force microscopy images

Acknowledgements TEQIP is gratefully acknowledged for providing instrumental facilities.

References

1. Shifler DA (2005) Corros Sci 47:2335
2. Corlet JL, Defranoux JM (1973) Corros Sci 13:575
3. Oldfield JW, Sutton WH (1978) Br Corros J 13:13
4. Oldfield JW, Sutton WH (1978) Br Corros J 13:104
5. Banday R, Cahoon JR (1977) Corrosion 33:204
6. Pessall N, Nurminen J (1974) Corrosion 30:381
7. Bond AP, Dundas JJ (1981) Corrosion 18:122
8. Turnbull A (1993) Br Corros J 28:297
9. Wilde BE, William E (1971) Electrochim Acta 16:1971
10. Brigham RJ (1989) Corros Sci 29:995
11. Dawson JL, Ferreira MG (1986) Corros Sci 26:1027
12. Darowicki K (2000) J Electroanal Chem 486:101
13. Darowicki K, Orliloowski J, Lentka G (2000) J Electroanal Chem 486:106
14. Darowicki K, Slepski P (2003) J Electroanal Chem 547:1
15. Darowicki K, Orliloowski J (2003) Electrochim Acta 50:2699
16. Bandy R, Van Rooyen D (1983) Corrosion 39:227
17. Lu YC, Bandy R, Clayton CR, Newman RC (1983) J Electrochem Soc 130:1774
18. Lu YC, Ives MB, Clayton CR (1993) Corros Sci 35:89
19. Kamachi Mudali U, Dayal PK, Gill TPS, Gnanamoorthy JB (1990) Corrosion 46:454
20. Oleford I, Wergrelius L (1995) Corros Sci 37:467
21. Sedriks AJ (1983) Int Mater Rev 28:306
22. Newman RC, Lu YC, Bandy R, Clayton CR (1984) Proceedings of the 9th International Congress on Metallic Corrosion. National Research Council, Toronto, p 394
23. Masimovitch S (1996) Electrochim Acta 41:2761
24. Magaino S, Matlosz M, Landolt D (1993) J Electrochem Soc 140:1365
25. Epelboin I, Gabrielli C, Keddam M, Takenoctli H (1975) Electrochim Acta 20:913
26. Alavi A, Cottis RA (1987) Corros Sci 27:443
27. Bastidas JM, Polo JL, Torres CL, Cano E (2001) Corros Sci 43:269
28. Nagarajan S, Rajendran N (2009) Corros Sci 51:217
29. Betova I, Bojinov M, Kinnunen P, Pohjanne P, Saario T (2002) Electrochim Acta 47:3335